Energy enhancements of gravity waves in the Antarctic lower stratosphere associated with variations in the polar vortex and tropospheric disturbances

Motoyoshi Yoshiki

Department of Geophysics, Faculty of Science, Kyoto University, Kyoto 606-8502, Japan[1]

Nobuhiko Kizu

Japan Meteorological Agency, Tokyo 100-8122, Japan

and

Kaoru Sato

National Institute of Polar Research, Tokyo 173-8515, Japan

Submitted to Journal of Geophysical Research in April 2004

Revised in September 2004

Accepted in September 2004

[1]now at National Institute for Environmental Studies, Tsukuba 305-8506, Japan

Abstract

Gravity waves in the Antarctic lower stratosphere are examined using original operational radiosonde data obtained at Syowa Station (69.0 °S, 39.6 °E) with fine vertical resolution. In the lower stratosphere, the temporal variation in gravity wave energy depends on height. In the height region of 13 – 15 km, just above the tropopause, the seasonal variation in gravity wave energy is not evident. The wave energy is rather enhanced when the absolute value of potential vorticity in the upper troposphere becomes small over Syowa Station. This fact implies that tropospheric disturbances affect the dynamical processes of gravity waves there. On the other hand, the gravity wave energy in the height region of 15 – 25 km shows clear seasonal variation having a maximum in spring. The time variation in gravity wave energy is examined in detail in terms of the polar vortex by using the equivalent latitude coordinate. Energy enhancements occur when the edge of the polar vortex approaches Syowa Station, and the enhancements are especially large when the polar vortex breaks down in spring. These results suggest that height variation in the background atmosphere leads to the difference of wave characteristics between the two height regions. The enhancements of wave energy are partly explained as modification of the wave structure by the background wind speed and the static stability, but it is also likely that enhancements of wave activity contribute to the energy enhancement at the edge of the polar vortex in spring.

1 Introduction

Gravity waves are now recognized to play an important role in the general circulation of the middle atmosphere. Gravity wave saturation and/or dissipation act as a force to accelerate or decelerate the background wind. This force not only alters the local wind but induces the meridional circulation in the middle atmosphere [e.g. Holton et al., 1995]. In the Antarctic winter, even in the lower stratosphere, temperature and wind fields are considered to be influenced by the dynamical forcing of gravity waves rather than planetary waves [Garcia and Boville, 1994].

To improve the understanding on interactions between gravity waves and the background atmosphere, it is important to examine temporal and spatial distribution of gravity wave characteristics. Since gravity waves have a wide range of vertical wave number, high resolution data obtained by observational tools such as radiosondes, radar, lidar, and remote sensors onboard a satellite are necessary to investigate the characteristics of gravity waves. There are many studies on the characteristics of gravity waves in middle and low latitude regions. Kitamura and Hirota [1989] examined the radiosonde data observed at northern midlatitudes to show a latitudinal and seasonal variation in gravity wave energy. Allen and Vincent [1995] also examined a latitudinal variation in gravity wave spectra using high resolution data obtained by radiosonde observations. These studies illustrated that seasonal variations in gravity wave energy show a maximum in winter at midlatitudes. The latitudinal variation that wave energy is larger at lower latitudes was also displayed. Furthermore, details of gravity wave characteristics at midlatitudes have been investigated in observational studies [e.g. Sato, 1994]. In the tropical stratosphere, both seasonal variation and the variation connected to the quasi-biennial oscillation (QBO) are observed in wave energy [Sato et al., 1994: Sato and Dunkerton, 1997; Vincent and Alexander, 2000]. Using data from Global Positioning System (GPS) Meteorology (GPS/MET) project, Tsuda et al. [2000] examined global distribution of wave energy and showed that similar variations are observed in satellite observations. However, both the climatology and the dynamical processes of gravity waves

in the polar regions are not yet well understood.

One of the observational studies of gravity waves in the polar regions is Yoshiki and Sato [2000], which examined gravity wave characteristics using radiosonde data obtained from many stations. They showed that wave characteristics are different between the Antarctic and the Arctic. In the Arctic lower stratosphere, potential energy of gravity waves is enhanced in winter at many stations. The wave energy correlates well with the surface wind. Hence it was inferred that gravity waves forced by orography are dominant in the Arctic. In the Antarctic, potential energy of gravity waves varies annually having a maximum in spring at many stations both on the coast of the Antarctica [Yoshiki and Sato, 2000] and inside of the Antarctica [Pfeninnger et al., 1999].

The observed variations in wave energy can arise from variation in both wave propagation and generation processes. In the polar lower stratosphere, the polar night jet is one candidate affecting these dynamical processes. Yoshiki and Sato [2000] suggested that the polar night jet plays an important role on the dynamical processes of gravity waves in the Antarctic lower stratosphere. They showed that the increase of static stability associated with the spring warming is related to potential energy enhancements in the Antarctic stratosphere. In the observational study in the Arctic, Whiteway et al. [1997] classified positions of the station relative to the polar vortex into three categories (i.e. the station is located inside, at the edge of, and outside the polar vortex) and examined the variation in wave energy in each category. They showed that larger wave energy is observed at the edge of the polar vortex than inside the vortex and that critical level filtering decides the energy variation at the vortex edge. Zink and Vincent [2001a, 2001b] emphasized the importance of the stratospheric wind. They showed that the seasonal march of potential energy correlates well with that of the background wind speed and suggested that the variation in wave energy can be reproduced by considering Doppler shifting effects without variations in wave sources. They argued that gravity waves having large phase speeds are important in the upper height region though their wave activity at a source level is small. This result is related to the limitation on the observable range of vertical wave numbers pointed out by Alexander [1998]. Meanwhile,

Sato et al. [1999] demonstrated that gravity waves are generated at the polar night jet through geostrophic adjustment in their experiment using a general circulation model.

Yoshiki and Sato [2000] focused their analysis on the climatological differences of wave characteristics between the Arctic and the Antarctic. In this study, temporal and height variations in wave characteristics in the Antarctic were examined in detail using original high quality data obtained by operational radiosonde observations at Syowa Station, which is located near the coast of the Antarctica. So as to investigate dynamical processes of gravity waves in the Antarctic lower stratosphere, we also examined the characteristics of background atmosphere commonly observed in case of the enhancement of wave energy. In section 2, details of the radiosonde data are described. Gravity wave characteristics, such as seasonal variation in wave energy and a dominant range of wave parameters are shown in section 3. We also focused our effort on illustrating the relation between gravity wave energy and the background field. Results are discussed in section 4. Concluding remarks are given in section 5.

2 Data Description

We have analyzed the temperature and horizontal wind data obtained by twice daily operational radiosonde observations at Syowa Station (69.0 °S, 39.6 °E) over a two year period from February 1997 to January 1999. As the original temperature data were sampled every four seconds and placed at irregular intervals in the vertical, we interpolated them linearly with an interval of 50 m to make the analysis easier. The horizontal wind data were calculated from the location of an ascending radiosonde. At first, the horizontal location of the radiosonde was obtained from the azimuth and the elevation angle of the tracking antenna at the station together with the altitude of the radiosonde. Next, horizontal wind data with an interval of one minute (about 300 meters in the vertical) were calculated from temporal differences of the sonde location. As the interval is not regular in the vertical due to the variation in the ascent speed of a radiosonde, we interpolated the wind data linearly with an

interval of 50 m in the vertical not to lose observed fine structure.

Note that the data analyzed in this study have much shorter sampling intervals than those analyzed in Yoshiki and Sato [2000]. The effective vertical resolution of temperature data is shorter than 100 m. In contrast, because of the smoothing in wind calculation, small vertical structure of horizontal wind are occasionally not resolved. While the amplitude of fluctuations with vertical wavelengths of less than 1 – 2 km are sometimes declined in the stratosphere, fluctuations with wavelengths longer than about 3 – 4 km are usually resolved adequately in wind data.

At Syowa station, observations are carried out continuously with few missing data. Furthermore, the height of a balloon burst is usually above 28 km despite low temperature in the lower Antarctic stratosphere in winter.

Gravity wave components of temperature and horizontal wind were extracted as follows: Four day running mean profiles are regarded as the background field at each height. We applied a bandpass filter with cut-off lengths of 2 and 8 km to vertical profiles of the deviation of the original time series from the background field. The obtained fluctuations are analyzed as gravity wave components.

3 Results

3.1 Temporal Variation in Gravity Wave Energy

Figure 1 shows the time-height sections of (a) zonal wind u, (b) temperature T, and (c) the Brunt-Väisälä frequency squared N^2 averaged over every 10 days in time and every 1 km in the vertical. The abrupt change in the Brunt-Väisälä frequency squared at the height of about 10 km corresponds to the tropopause. Except in summer, the polar night jet is observed in the height region of 15 – 30 km. As the surface wind is easterly, there is a critical level for orographically-forced gravity waves at the height of about 3 km. In the height region of 15 – 25 km, the temperature falls extremely low in winter. In spring, warming occurs earlier at

Fig. 1

higher altitudes and the region of high static stability propagates downward. Simultaneously the polar night jet in the stratosphere begins to decelerate from the upper height and the region of the maximum wind speed also descends in time.

Figure 2 shows the time height sections of (a) potential energy (PE $\equiv (g^2/2N^2)(\overline{T'^2}/T^2)$) and (b) kinetic energy (KE $\equiv (1/2)(\overline{u'^2 + v'^2})$) of gravity waves per unit mass averaged in the same way as in Figure 1, where g is the gravitational acceleration, v the meridional wind, prime the gravity wave component defined in section 2, over-bar the average in time. In the stratosphere, potential energy varies annually increasing in winter and spring. In the height region of 15 – 25 km, potential energy has a maximum in spring, when the region of high static stability propagates downward. These results agree well with the climatology obtained by Yoshiki and Sato [2000]. However, the close examination of the seasonal variation in each year reveals that potential energy has a peak in particular time periods namely, November 1997, October and December 1998 even when the static stability begins to decrease in the height region of 20 – 25 km. The temporal and spatial variations observed in kinetic energy are similar to those of potential energy in the lower stratosphere. Fig. 2

Then we divided the lower stratosphere into two height regions: One is the height region of 15 – 25 km, where the spring enhancement of gravity wave energy is clearly observed. The other is the height region of 13 – 15 km, where seasonal variation in wave energy is not evident. The lower limit of the latter region was determined to avoid contamination by the tropopause. The height region above 25 km is not analyzed here due to the insufficient significant data.

Figure 3 illustrates the potential energy averaged over the height regions of (a) 20 – 22 km and (b) 13 – 15 km. We took an average in the same height interval for the upper and lower regions. Five point running mean was applied to both time series (the thin curves). To represent the seasonal variation clearly, the time series with 31 point running mean are also displayed in the thick curves. As examined in Figure 2, in the height region of 20 – 22 km, the seasonal variation is clear having a maximum in spring and the second peak in autumn. Remarkable enhancements are observed in September and November in 1997, September, Fig. 3

October and December in 1998. In the height region of 13 – 15 km, the seasonal variation in potential energy is not clear. Instead, it is noteworthy that potential energy often shows enhancements with timescales less than 10 days throughout the data period.

The time series of (a) wind speed and (b) Brunt-Väisälä frequency squared averaged in the same height regions are shown in Figure 4 for comparison with potential energy. The thin solid and thin dashed curves denote the time series in the height regions of 20 – 22 km and 13 – 15 km, respectively, to which five point running mean is applied. The time series with 31 point running mean are also displayed by thick solid curves for the height region of 20 – 22 km and thick dashed curves for the height region of 13 – 15 km, respectively. In both height regions, wind speed varies annually showing enhancements from autumn to spring. The wind speed is larger in the height region of 20 – 22 km and has a maximum in September 1997 and October 1998. Large variations in wind speed are observed from July to November in 1997, while wind speed becomes large gradually from July to October in 1998. The Brunt-Väisälä frequency squared also shows seasonal variation having a maximum in October 1997 and October 1998 in the height region of 20 – 22 km, while the seasonal variation is relatively small in the height region of 13 – 15 km. In the height region of 20 – 22 km, the Brunt-Väisälä frequency squared rises sharply in early October in 1997, while it becomes large gradually in 1998.

Fig. 4

The observed potential energy often correlates well with the background fields in the upper height. In the height region of 20 – 22 km, both potential energy and wind speed are large from autumn to spring. Furthermore, enhancements of potential energy and wind speed occur simultaneously in autumn (May 1997 and May 1998) and spring (September 1997 and October 1998). The spring enhancement of potential energy also coincides with the increase of the Brunt-Väisälä frequency in spring. However, it is noteworthy that the remarkable maxima of potential energy in November 1997 and December 1998 do not have the corresponding peaks in wind speed and the Brunt-Väisälä frequency. The wind speed and the Brunt-Väisälä frequency rather began to decrease at these periods.

So as to examine the enhancement of wave energy as a function of vertical wave number,

monthly mean vertical wave number spectra of normalized temperature T'/T are calculated in the height region of 15 – 25 km. The spectra were calculated from the deviation of the original profile from the background field defined in section 2. Figure 5 shows the monthly mean vertical wave number spectrum in an energy-content form for February, May, August, November 1997, respectively. The thin curves denote the observed spectrum, while the model spectrum $N^4/(10g^2m^3)$ by Smith et al. [1987] is also plotted in long-dashed lines as a reference, since this model spectrum generally well explains observations in the midlatitudes. The model spectrum assumes gravity waves whose amplitude is limited by saturation. As shown in the equation, the power spectrum density of the model spectrum is proportional to N^4.

Fig. 5

From Figure 5, it is shown that the dominant vertical wave number of gravity waves is 2 – 5 $\times 10^{-4}$ m^{-1}, corresponding to the wavelength of about 2 – 5 km, in every month. In the wave number region lower than 2×10^{-3} m^{-1}, the power spectrum density is generally less than that of the model spectrum. Nonetheless, the slope of the spectrum seems to be approximately constant except in November 1997, which implies that the power spectrum density in the low wave number region varies depending on static stability. In November 1997, when remarkable increases of potential energy are observed in Figure 3, enhancements of power spectrum density seem to occur in a wide range of the low wave number region.

3.2 Wave Characteristics Estimated by Hodograph Analysis

In order to examine gravity wave parameters, such as directions of wave propagation and ground-based phase speed, vertical variations in horizontal wind vectors (hodograph) of gravity wave components were examined in the height regions of 13 – 15 km and 15 – 25 km. For hydrostatic monochromatic inertia-gravity waves, horizontal wind fluctuations parallel to the wave number vector U', those perpendicular to the wave number vector V', and normalized temperature fluctuations T'/T satisfy the following polarization relations:

$$U' = \mathrm{Re}[\frac{\widehat{\omega}kA}{\sqrt{\widehat{\omega}^2 - f^2}} \exp i(mz + \phi_0)], \tag{1}$$

$$V' = \mathrm{Re}[\frac{-ifkA}{\sqrt{\widehat{\omega}^2 - f^2}} \exp i(mz + \phi_0)], \tag{2}$$

$$\frac{T'}{T} = \mathrm{Re}[\frac{imA}{g} \exp i(mz + \phi_0)], \tag{3}$$

where i is the imaginary unit, Re[ ] the real part of a complex number, k the horizontal wave number, m the vertical wave number, $\widehat{\omega}$ the intrinsic frequency, z the altitude, A a constant of amplitude, and ϕ_0 a constant phase at $z = 0$, respectively. Equations (1) and (2) reveal that gravity wave parameters can be estimated by fitting an observed hodograph of gravity wave components to an ellipse under the assumption that fluctuations are locally due to an inertia-gravity wave. [Hirota and Niki, 1985; Sato, 1994]. The associated temperature fluctuation is also used to remove the ambiguity in the horizontal direction of wave propagation. The vertical wave number m, the horizontal direction of wave propagation relative to the background wind, and the ratio of short to long axes of the ellipse b/a were estimated from the gravity wave component defined in section 2, where a is the length of the long axis and b is that of the short axis of the ellipse fitted to the hodograph, respectively.

Details of the procedure of the analysis is similar to that applied in Yoshiki and Sato [2000]. The height interval of the data used in each fitting was selected as two kilometers and the interval was slid by 500 m for each fitting.

The statistics were made for cases in which the ratio b/a is from 0.1 to 0.9 (i.e. $(10/9)f < \widehat{\omega} < 10f$) and the kinetic energy KE > 1 J kg^{-1}. If the fluctuations are due to internal gravity waves, the phase constant of a sinusoidal curve fitted to temperature fluctuations ϕ_T should be equal to that of wind fluctuations ϕ_V as expressed in ϕ_0 of Equations (1) – (3). Thus the wave parameters were estimated only when $|\phi_T - \phi_V| < 0.5$ radian (corresponding to about 30 degrees). Another threshold is that the ratio of the mean square of the residuals of fitting to the kinetic energy is less than 0.5.

Figure 6 shows the histogram of vertical wavelength. The left and right panels are the results for the height regions of 13 – 15 km and 15 – 25 km in summer (from December to February, denoted later as DJF; upper panels), autumn (from March to May, denoted as MAM; second panels), winter (from June to August, denoted as JJA; third panels), and

Fig. 6

spring (from September to November, denoted as SON; lower panels), respectively. The open columns denote the probability density of gravity waves transferring energy upward, while the shaded columns denote the probability density of gravity waves transferring energy downward. The numbers written in the right-upper corner of each panel denote the number of data used in the statistics and the percentage of gravity waves transferring energy downward.

In the height regions of both 13 – 15 km and 15 – 25 km, the dominant vertical wavelength is about 3 – 4 km, which reflects the transfer function of the band-pass filter. The percentage of gravity waves transferring energy downward shows interesting seasonal variation. Gravity waves transferring energy downward are dominant in winter in the upper height region, while the percentage of them is small in summer and autumn. In spring, when gravity wave energy has a maximum, the percentage of gravity waves transferring energy downward decreases, though it is still large compared with summer and autumn.

Figure 7 shows the histogram of the inverse number of intrinsic frequencies multiplied by the Coriolis parameter $f/\widehat{\omega}$, which is equivalent to the ratio of short to long axes of the fitted ellipse b/a. In the height regions of both 13 – 15 km and 15 – 25 km, gravity waves of high intrinsic frequencies (i.e. small $f/\widehat{\omega}$) are frequently observed in winter and spring. Fig. 7

Next, horizontal wavelength is calculated from the horizontal wave number k estimated using the dispersion relation of a hydrostatic inertia-gravity wave,

$$\frac{k^2}{m^2} = \frac{\widehat{\omega}^2 - f^2}{N^2}. \tag{4}$$

The histogram of horizontal wavelength is shown in Figure 8. In summer, the dominant horizontal wavelength is about 500 km both in the height region of 13 – 15 km and 15 – 25 km. From autumn to spring, gravity waves having horizontal wavelength shorter than 500 km are dominant in both height regions. Fig. 8

Then, horizontal directions of wave propagation and ground-based phase speed are examined. As the ground-based frequency ω is related to the intrinsic frequency $\widehat{\omega}$ by

$$\omega = \widehat{\omega} + \mathbf{U} \cdot \mathbf{k}, \tag{5}$$

the ground-based phase speed $\mathbf{c}$ is described as

$$\mathbf{c} = (\widehat{\omega} + \mathbf{U} \cdot \mathbf{k}) \frac{\mathbf{k}}{|\mathbf{k}|^2}. \tag{6}$$

Figures 9 and 10 illustrate the probability density of the directions of wave propagation relative to the mean wind and the directions of ground-based phase speed, respectively. The thin dashed curves denote the results for summer (DJF), the thick dashed curves for autumn (MAM), the thin solid curves for winter (JJA), and the thick solid curves for spring (SON), respectively.

Fig. 9

Fig. 10

In Figure 9, it seems that the horizontal direction of wave propagation is slightly different between the height regions of 13 – 15 km and 15 – 25 km. From autumn to spring, gravity waves propagate westward relative to the mean wind in the height region of 15 – 25 km and westward and north-westward relative to the mean wind in the height region of 13 – 15 km. On the other hand, the dominant direction of ground-based phase speed observed in Figure 10 is eastward from autumn to spring in both height regions. Thus, gravity waves are significantly Doppler-shifted. This is consistent with the increase of the number of gravity waves having high intrinsic frequencies observed in Figure 7.

The histogram of ground-based phase speed is also shown in Figure 11. In the height region of 13 – 15 km, gravity waves having small phase speeds near zero are dominant in all seasons. Note that orographically-forced waves are not able to propagate from the surface except in summer due to a critical level in the lower troposphere. In the height region of 15 – 25 km, the dominant ground-based phase speed is about 10 – 20 m s^{-1} in summer. From autumn to winter, gravity waves having smaller phase speeds have larger probability densities. However, it is also noteworthy that the probability density of gravity waves having large phase speeds increases in winter and spring in the height region of 15 – 25 km compared with the height region of 13 – 15 km.

Fig. 11

Then, to examine the upward propagation of gravity waves, characteristics of gravity waves at energy enhancements in the height region of 13 – 15 km were analyzed. Figure 12 shows the probability density of gravity waves whose potential energy in the height region of

Fig. 12

13 – 15 km is greater than 1.5 J kg^{-1} as a function of ground-based phase speed. Shaded and open columns indicate the case when the potential energy is larger and less than 1.5 J kg^{-1} in the height region of 20 – 22 km.

It is clear that potential energy in the upper height region becomes large only when the phase speed of gravity waves in the lower region is small. This implies that only gravity waves having small phase speeds propagate upward. Since the wind speed is about 20 m s^{-1} in the height region of 13 – 15 km and larger than 50 m s^{-1} in the height region of 20 – 22 km as observed in Figure 4a, gravity waves having phase speeds larger than 20 m s^{-1} would meet critical levels or dissipate during the upward propagation.

3.3 Common Characteristics of the Background Field when Gravity Waves Have Large Amplitude

As examined in section 3.1, the temporal variation in gravity wave energy depends on height in the lower stratosphere: While seasonal variation in potential energy is dominant in the height region of 15 – 25 km, energy enhancements with short duration are often observed in the height region of 13 – 15 km.

Figure 13 shows typical examples of potential vorticity (PV) on an isentrope of 300 Kelvin (corresponding to the height of about 7 – 8 km) when gravity wave energy shows enhancements in the height region of 13 – 15 km. The examples are shown for June 19, 1997 and March 20, 1998. The closed circle denotes the location of Syowa Station. In general, the absolute value of PV is larger at higher latitudes. However, the absolute value of PV at Syowa Station becomes small on both days. On June 19, 1997, low PV penetrates into not only the coast but the inside of the Antarctica due to blocking caused by quasi-stationary Rossby waves [Hirasawa et al., 2000]. On March 20, 1998, low PV due to wavy structure of synoptic-scale disturbances is observed near Syowa Station. Fig. 13

Figure 14 shows (a) the histogram of PV on an isentrope of 300 Kelvin at Syowa Station and (b) the composite of the time series of PV. The shaded columns in Figure 14a denote the Fig. 14

probability density of gravity waves as a function of PV whose potential energy is more than 1.5 J kg^{-1} in the height region of 13– 15 km, while the open columns denote the probability density for all period. To calculate the composite in Figure 14b, we define a key day (lag $= 0$ in the abscissa) as the day when potential energy in the height region of 13 – 15 km is larger than 1.5 J kg^{-1}. It is clear that the absolute value of PV is small when gravity wave energy has large potential energy. Furthermore, the absolute value of PV begins to decrease rapidly from the time lag of -1 day and has a peak around the time lag of 2 days. The observed slight delay of the PV minimum implies that wave energy is enhanced in the area downstream of the ridge in the upper troposphere.

Next, the relation between gravity wave energy in the upper height region and the polar vortex was examined. So as to examine the developing and decaying processes of the polar vortex as a whole, the definition of the polar night jet on equivalent latitude coordinate [Nash et al., 1996] was adapted in this analysis. The equivalent latitude is defined as the latitude whose latitude circle covers the same area as a PV contour encloses. As the polar vortex and PV contours are distorted by planetary waves in similar shape, PV is useful as a latitude coordinate to represent the position relative to the polar vortex. On the equivalent latitude coordinate, the edge of the polar vortex was defined as the location of the highest PV gradient.

Results for the year of 1997 are shown in Figure 15. Figure 15a shows the time-latitude section of PV gradient on an isentrope of 480 Kelvin (about 18 km). The closed circles in Figure 15a denote the equivalent latitude of the jet axis, while the solid curve denotes the equivalent latitude calculated from potential vorticity at Syowa Station. In Figure 15b, potential energy of gravity waves (the solid curve) and wind speed (the dotted curve) averaged over the height region of 15 – 25 km at Syowa Station are displayed. Fig. 15

In winter and early spring, Syowa Station is located usually at a higher latitude than the polar night jet. In late spring, the equivalent latitude of Syowa Station begins to show large variations and the polar night jet sometimes approaches Syowa Station, as planetary waves are amplified in the stratosphere. In November 1997, the polar vortex breaks down

corresponding to the disappearance of the large latitudinal gradient of PV. The polar night jet approaches Syowa Station three times in the periods of 8, 11 – 18, and 24 – 28 November. It is noteworthy that large energy enhancements occur when the polar vortex breaks down and the vortex edge is located in the vicinity of Syowa Station. In contrast, on 10 and 20 November, when potential energy is small, the equivalent latitude of the station departs from that of the polar night jet. In September, potential energy also shows enhancements when the jet approaches Syowa Station. Since local wind speed increases when the polar night jet approaches Syowa station, wind speed is also highly correlated with potential energy. However, the maximum of wind speed in November is rather smaller than that in September.

Results for spring in 1998 are shown in Figure 16. The equivalent latitude of the polar night jet decreases gradually in spring, while it decreases eventually in 1997. The disappearance of the large latitudinal gradient of PV indicates that the polar vortex breaks down in December. The time of the final warming of the stratosphere is different from that in 1997. However, the energy enhancement observed in December 1998 is similar to that in November 1997 in a sense that potential energy becomes large when the polar vortex breaks down and the edge of the vortex approaches Syowa Station. Potential energy also becomes large in October, when the polar night jet approaches Syowa Station.

Fig. 16

4 Discussion

4.1 Energy Enhancement at the Edge of the Polar Vortex

As examined in section 3.1, potential energy of gravity waves shows seasonal variation having a maximum in spring in the height region of 15 – 25 km, while the seasonal variation is not clear below the height of 15 km. In the height region of 15 – 25 km, the remarkable enhancement of wave energy is observed at the edge of the polar vortex when the polar vortex breaks down in spring. Here, we discuss the dynamical mechanisms of the energy enhancement in spring.

Potential energy of gravity waves varies through the change of the background field and wave activity. From the polarization relation and the dispersion relation of hydrostatic inertia-gravity waves, potential energy PE is described as

$$\text{PE} = \frac{1}{2}\frac{N}{\widehat{\omega}}(1 - \frac{f^2}{\widehat{\omega}^2})^{-1/2}F_z, \tag{7}$$

where $F_z \equiv (1 - f^2/\widehat{\omega}^2)\overline{U'W'}$ is the pseudo-momentum flux of inertia-gravity waves [Fritts and Vincent, 1987], U' the horizontal wind component of gravity waves parallel to the wave number vector, and W' the vertical wind component of gravity waves, respectively. Thus, potential energy varies depending on the Brunt-Väisälä frequency N, the intrinsic frequency $\widehat{\omega}$, and the pseudo-momentum flux F_z.

From Equation (7), it is shown that potential energy increases when the Brunt-Väisälä frequency becomes large. As examined in section 3.1, the Brunt-Väisälä frequency varies annually having a maximum in October 1997 and September 1998. This may be consistent with the observation that both static stability and wave energy become large in spring. However, the large energy enhancements are observed in November 1997, and December 1998, when the static stability begins to decrease. Thus, the high static stability alone cannot explain the energy enhancements in late spring.

Equation (7) also shows that potential energy increases when the intrinsic frequency of gravity waves decreases. Thus, the observed positive correlation between potential energy and the wind speed may be attributed to Doppler shifting effects, except for waves whose direction of propagation is perpendicular to the wind direction. In section 3.2, it is shown that gravity waves propagating upstream relative to the mean wind are dominant from winter to spring. Assuming ground-based frequency is constant, potential energy should decrease with the enhancement of the wind speed. Thus, the observed variation in Figures 15 and 16 is not likely to be explained by Doppler shifting effects.

As it is difficult to explain the observed potential energy variation by the variation in intrinsic frequency and the Brunt-Väisälä frequency, we need to attribute the observed enhancements of potential energy to the increase of the momentum flux.

Assuming gravity waves propagating vertically, one candidate causing the variation in momentum flux is critical level filtering of waves propagating upward. From autumn to spring, wind speed is usually about 20 m s^{-1} in the height region of 13 – 15 km and increases with height. As the dominant ground-based phase speed in the height region of 13 – 15 km is less than 20 m s^{-1} in both winter and spring, the contribution of critical level filtering seems small in both winter and spring. Thus, critical level filtering would not explain the difference of potential energy between winter and spring.

It is possible that the spring maximum of potential energy is caused by strong gravity wave sources. Sato et al. [1999] showed dominance of downward propagating gravity waves around the polar night jet in their experiment using a general circulation model. Sato [2000] discussed these waves are possibly generated through geostrophic adjustment. In late spring, when the vortex is largely distorted and breaks down, wave energy can be enhanced as a result of wave generation at the edge of the polar vortex.

As examined in Figure 10, gravity waves having ground-based phase speeds larger than the wind speed in the height region of 13 – 15 km are observed in the height region of 15 – 25 km. These waves cannot propagate upward from the tropopause because they meet a critical level during the upward propagation as examined in Figure 12. This result also implies the existence of wave sources in the upper height region in winter and spring.

4.2 Gravity Waves Slightly above the Tropopause

In the height region of 13 – 15 km, energy enhancements are observed when low potential vorticity in the upper troposphere approaches Syowa Station throughout the data period. It suggests that gravity wave energy is enhanced near the ridge in the upper troposphere associated with tropospheric vorticities such as synoptic-scale disturbances. Similar energy enhancements associated with tropospheric disturbances are observed in many studies so far [e.g. Uccellini and Koch, 1987].

So as to investigate gravity waves associated with baroclinic waves, O'Sullivan and

Dunkerton [1995] made an numerical experiment and showed that gravity waves are generated by geostrophic adjustment at the tropopause during the growth of synoptic-scale waves. Sato [1989] examined the wind data obtained by a Mesosphere, Stratosphere, and Troposphere (MST) radar and showed that gravity waves are generated at the tropopause. While these two studies pay an attention to gravity waves generated in association with synoptic-scale trough passage at the tropopause, Guest et al. [2000] showed that gravity waves in the stratosphere are likely to be generated at the front near the surface under similar synoptic patterns by applying a ray tracing method to high resolution radiosonde data at Macquarie Island (55 °S).

Gravity waves observed just above the tropopause at Syowa Station are similar to those observed in these studies, having frequencies near the inertia frequency f. The gravity wave energy in the height region of 13 – 15 km becomes large in June 19, 1997, when a blocking occurs and low potential vorticity penetrates into the Antarctica. This may imply that geostrophic adjustment is important for the enhancements of wave energy.

A recent study by Shibata et al. [2003] showed the case that gravity waves in the lower stratosphere at Syowa Station are associated with a decaying process of tropospheric disturbances, and temperature fluctuations due to the observed waves lead to the formation of Polar Stratospheric Clouds (PSCs). Not only the orographically-forced waves as pointed out by former studies [e.g. Carslaw et al., 1998], but gravity waves associated with tropospheric disturbances are also important for chemical processes in the Antarctic lower stratosphere.

5 Concluding Remarks

Gravity waves in the Antarctic lower stratosphere are examined using operational radiosonde data observed at Syowa Station (69.0 °S, 39.6 °E). In the lower stratosphere, it was shown that gravity wave energy and wave characteristics depend on height.

In the height region of 13 – 15 km, just above the tropopause, energy enhancements with short duration are frequently observed when low potential vorticity in the troposphere

approaches Syowa Station. Tropospheric disturbances, such as synoptic-scale disturbances and blocking may contribute to the generation of gravity waves.

In the height region of 15 – 25 km, gravity wave energy varies annually having a maximum in spring. The energy enhancement is especially large when the polar vortex breaks down and the edge of the vortex approaches the station in spring. As it is difficult to explain the energy enhancements only by the variation in horizontal wind and/or the static stability, the enhancements of wave activity at the edge of the polar vortex are likely to contribute to the energy enhancements by wave generation in the stratosphere.

Though the connection between the energy enhancements and the position relative to the polar vortex is observed both in 1997 and 1998, the data period analyzed in this study is not long enough to examine interannual variations. Thus, it is not evident whether the enhancements of wave energy at the edge of the polar vortex occur constantly in every spring. In fact, Figures 15 and 16 show that the enhancements of potential energy are quite different between 1997 and 1998. Following the discussion in section 4.1, interannual variation of the stratospheric circulation in the Southern Hemisphere may cause large variation in the enhancements of potential energy.

Not only the enhancements in spring, seasonal variation in gravity wave energy also differs between 1997 and 1998 as observed in Figures 2 and 3. In addition, Yoshiki and Sato [2000] shows that the energy enhancement in spring does not occur simultaneously in the Antarctic but depends on the seasonal march of the stratospheric circulation at each station. It is important to investigate the variation in gravity wave characteristics from viewpoint of the connection with the stratospheric circulation in the Southern Hemisphere.

Acknowledgements

We are grateful to Mr. T. Suita of Japan Meteorological Agency for the provision of radiosonde data from February 1998 to January 1999. GFD-DENNOU Library is used for drawing figures.

References

Alexander, M. J., Interpretations of observed climatological patterns in stratospheric gravity wave variance, *J. Geophys. Res.*, *103*, 8,627 – 8,640, 1998.

Allen, S. J., and R. A. Vincent, Gravity wave activity in the lower atmosphere: Seasonal and latitudinal variations, *J. Geophys. Res.*, *100*, 1,327 – 1,350, 1995.

Carslaw, K. S., Wirth M., Tsias A., Luo B. P., Dornbrack A. Leutbecher M. Volkert H., Renger W., Bacmeister J. T., Reimer E., and Peter Th., Increased stratospheric ozone depletion due to mountain-induced atmospheric waves, *nature*, *391*, 675 – 678, 1998.

Fritts, C. D., and R. A. Vincent, Mesospheric momentum flux studies at Adelaide, Australia: Observations and a gravity wave-tidal interaction model. *J. Atmos. Sci*, *44*, 605 – 619, 1987.

Garcia, R. R, and B. A. Boville, "Downward Control" of the mean meridional circulation and temperature distribution of the polar winter stratosphere, *J. Atmos. Sci.*, *51*, 2,238 – 2,245, 1994.

Guest, F. M., M. J. Reeder, C. J. Marks, and D. J. Karoly, Inertia-gravity waves observed in the lower stratosphere over Macquarie Island, *J. Atmos. Sci.*, *57*, 737 – 752, 2000.

Hirasawa, N., H. Nakamura, and T. Yamanouchi, Abrupt changes in meteorological conditions observed at an inland Antarctic station in association with wintertime blocking, *Geophys. Res. Lett.*, *27*, 1,911 – 1,914, 2000.

Hirota, I., and T. Niki, A statistical study of inertia-gravity waves in the middle atmosphere, *J. Meteor. Soc. Japan*, *63*, 1,055 – 1,066, 1985.

Holton, J. R., P. H. Haynes, M. E. McIntyre, A. R. Douglass, R. B. Rood, and L. Pfister, Stratosphere-troposphere exchange, *Revi. of Geophs.*, 33, 403 – 439, 1995.

Kitamura, Y., and I. Hirota, Small-scale disturbances in the lower stratosphere revealed by daily rawin sonde observations, *J. Meteorol. Soc. Jpn., 67*, 817 – 831, 1989.

Nash, E. R., P. A. Newman, J. E. Rosenfield, and M. R. Schoeberl, An objective determination of the polar vortex using Ertel's potential vorticity, *J. Geophys. Res., 101*, 9,471 – 9,478, 1996.

O'Sullivan, D., and T. J. Dunkerton, Generation of inertia-gravity waves in a simulated life cycle of baroclinic instability, *J. Atmos. Sci., 52*, 3,935 – 3,716, 1995.

Pfenninger, M., A. Z. Liu, G. C. Papem and C. S. Gardner, Gravity wave characteristics in the lower atmosphere at South Pole, *J. Geophys. Res., 104*, 5,963 – 5,984, 1999.

Sato, K., An inertial gravity wave associated with a synoptic-scale pressure trough observed by the MU radar, *J. Meteorol. Soc. Jpn, 67*, 325 – 334, 1989.

Sato, K., A statistical study of the structure, saturation, and sources of inertia-gravity waves in the lower stratosphere observed with the MU radar, *J. Atmos. Terr. Phys., 56*, 755 – 774, 1994.

Sato, K., Sources of gravity waves in the polar middle atmosphere, *Adv. Polar Upper Atm. Res., 14*, 233 – 240, 2000.

Sato, K., T. J. Dunkerton, Estimates of momentum flux associated with equatorial Kelvin and gravity waves, *J. Geophys. Res., 102*, 26,247 – 26,261, 1997.

Sato, K., F. Hasegawa, and I. Hirota, Short-period disturbances in the equatorial lower stratosphere, *J. Meteorol. Soc. Jpn., 72*, 859 – 872, 1994.

Sato, K., T. Kumakura, and M. Takahashi, Gravity waves appearing in high-resolution GCM simulation, *J. Atmos. Sci., 56*, 1,005 – 1,018, 1999.

Shibata, T., K. Sato, H. Kobayashi, M. Yabuki, and M. Shiobara, Antarctic polar stratospheric clouds under temperature perturbation by nonorographic inertia gravity waves

observed by micropulse lidar at Syowa Station, *J. Geophys. Res.*, *108*, 4105, doi:10.1029/2002JD002713, 2003.

Smith, S. A., D. C. Fritts, and T. E. VanZandt, Evidence for saturated spectrum of atmospheric gravity waves, *J. Atmos. Sci.*, *44*, 1,404 – 1,410, 1987.

Tsuda, T., M. Nishida, C. Rocken, and R. H. Ware, A global morphology of gravity wave activity in the stratosphere revealed by the GPS occultation data (GPS/MET), *J. Geophys. Res.*, *105*, 7,257 – 7,273, 2000.

Uccellini, L. W., and S. E. Koch, The synoptic setting and possible energy sources for mesoscale wave disturbances, *J. Atmos. Sci.*, *115*,721 – 729, 1987.

Yoshiki, M., and K. Sato, A statistical study of gravity waves in the polar regions based on operational radiosonde data, *J. Geophys. Res.*, *105*, 17,995 – 18,011, 2000.

Vincent, R. A., and M. J. Alexander, Gravity waves in the tropical lower stratosphere: An observational study of seasonal and interannual variability, *J. Geophys. Res*, *105*, 17,971 – 17,982, 2000.

Whiteway, J. A, T. J. Duck, D. P. Donovan, J. C. Bird, S. R. Pal, and A. I. Carswell, Measurements of gravity wave activity within and around the Arctic stratospheric vortex, *Geophys. Res. Lett.*, *24*, 1,387 – 1,390, 1997.

Zink, F., and R. A. Vincent, Wavelet analysis of stratospheric gravity wave packets over Macquarie Island 1. Wave parameters, *J. Geophys. Res.*, *106*, 10,275 – 10,288, 2001a.

Zink, F., and R. A. Vincent, Wavelet analysis of stratospheric gravity wave packets over Macquarie Island 1. Intermittency and mean-flow accelerations, *J. Geophys. Res.*, *106*, 10,289 – 10,297, 2001b.

List of Figures

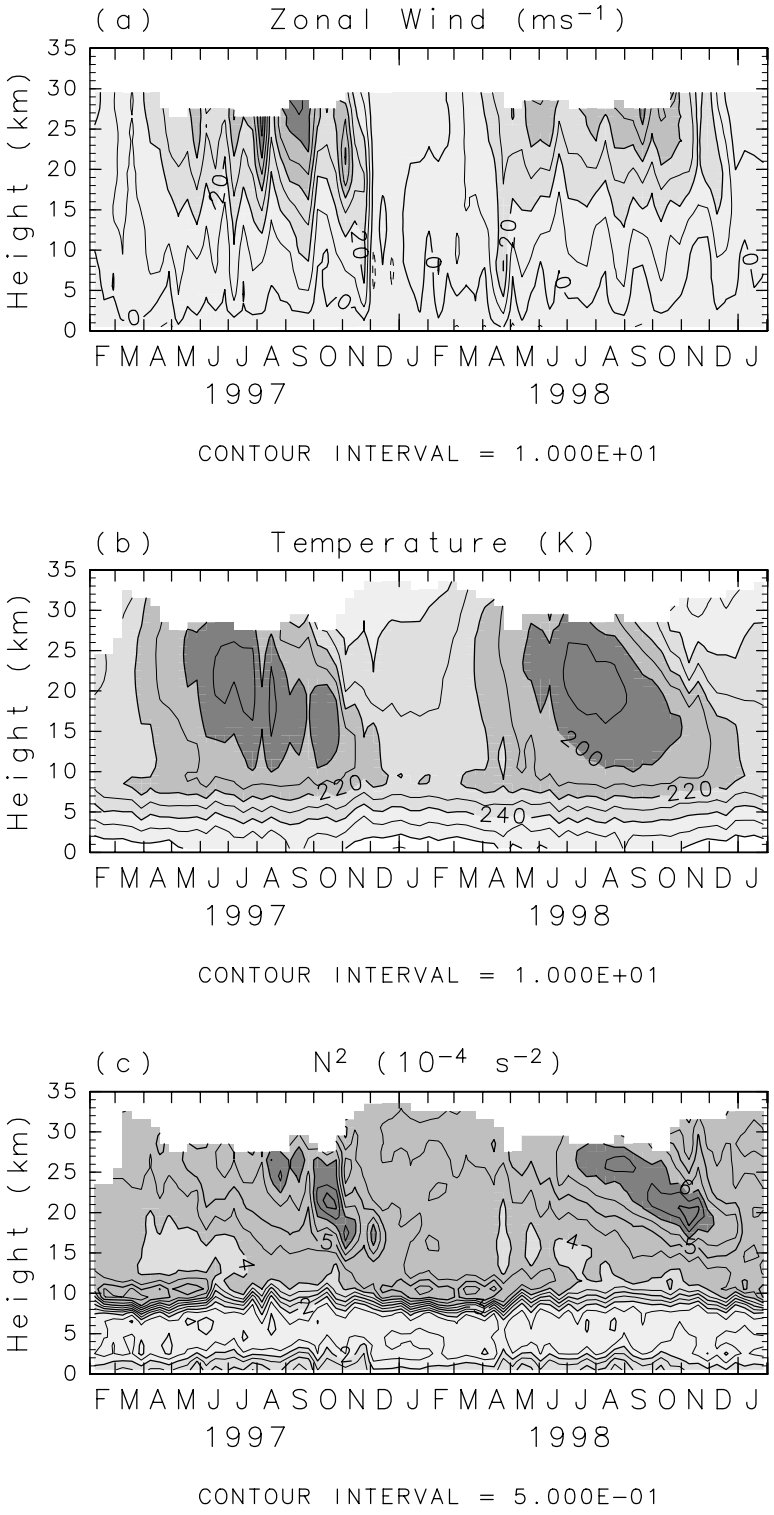

Figure 1: The time-height sections of (a) zonal wind u (m s^{-1}) (b) temperature T (K) (c) the Brunt-Väisälä frequency squared N^2 (s^{-2}) averaged over 10 days in time and 1 km in the vertical at Syowa Station. The contour intervals are 10 m s^{-1}, 10 K, 5×10^{-5} s^{-2}, respectively.

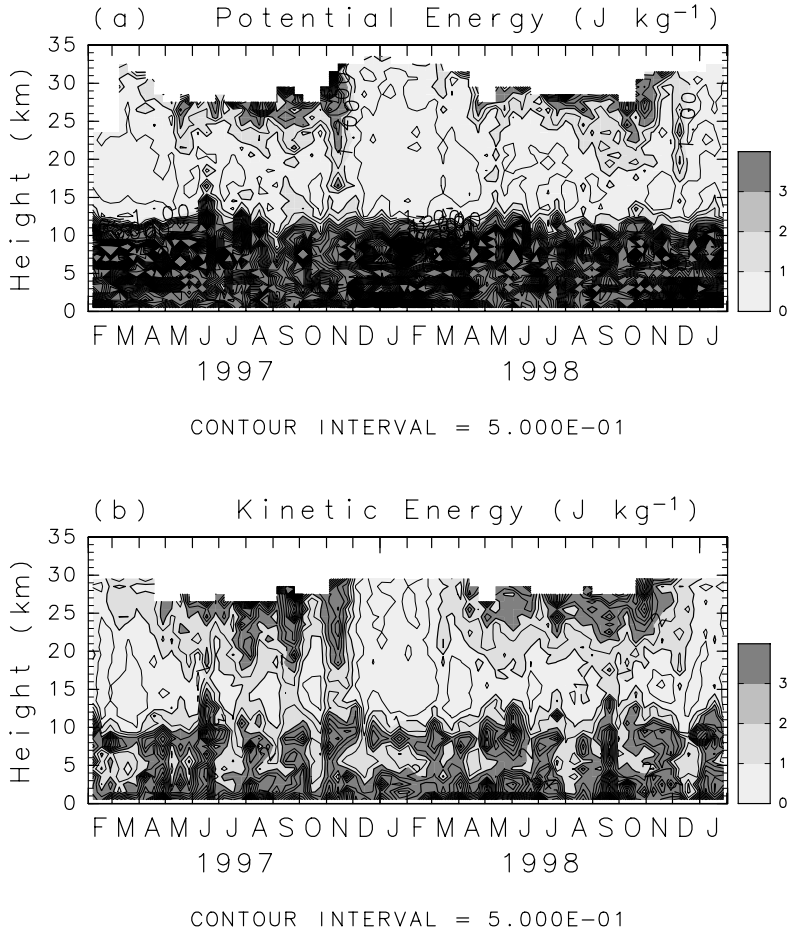

Figure 2: The time-height sections of (a) potential energy and (b) kinetic energy of gravity waves at Syowa station. The unit is J kg^{-1}. The contour interval is 0.5 J kg^{-1}.

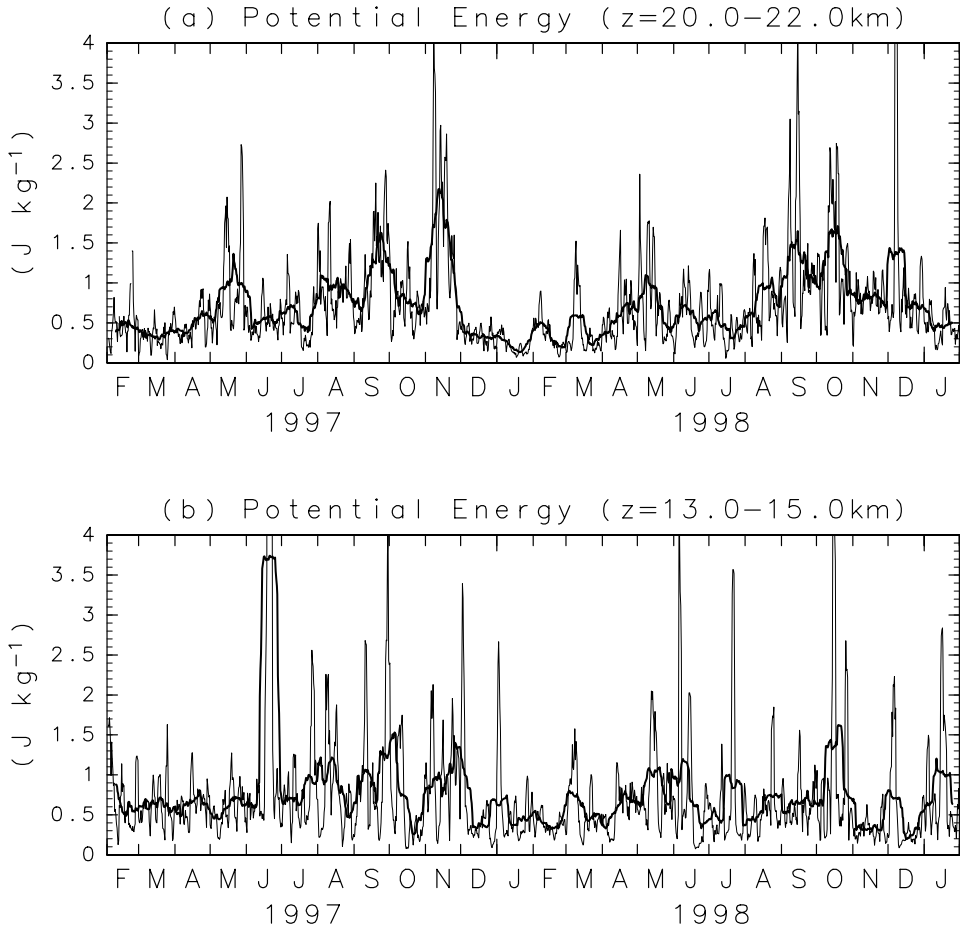

Figure 3: The time series of potential energy averaged over the height regions of (a) 20 – 22 km and (b) 13 – 15 km, respectively. The thin and the thick curves denote the time series with 5 and 31 points running mean, respectively. The unit is J kg^{-1}.

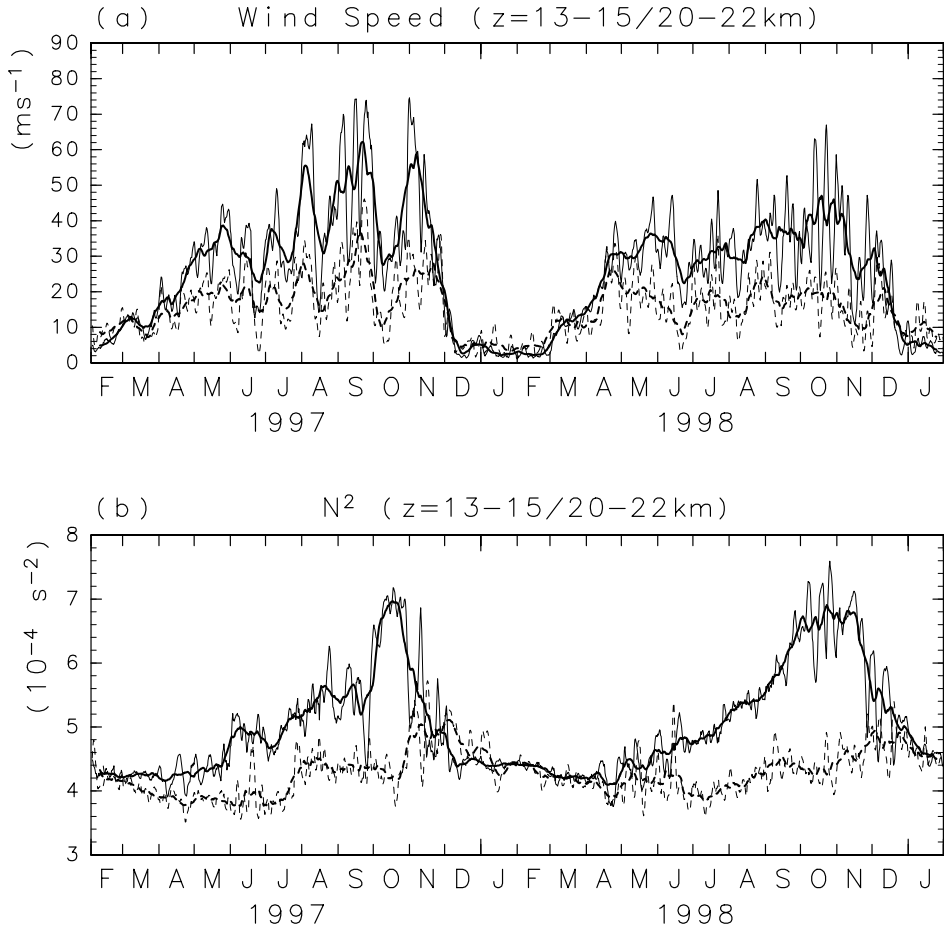

Figure 4: The time series of (a) wind speed u (m s^{-1}) and (b) Brunt-Väisälä frequency squared N^2 ($10^{-4}\times$ s^{-2}) averaged in the height regions of 20 – 22 km and 13 – 15 km. The thin and the thick solid curves denote the time series with 5 and 31 points running mean respectively in the height region of 20–22 km, while the thin and the thick dashed curves denote the results in the height region of 13–15 km.

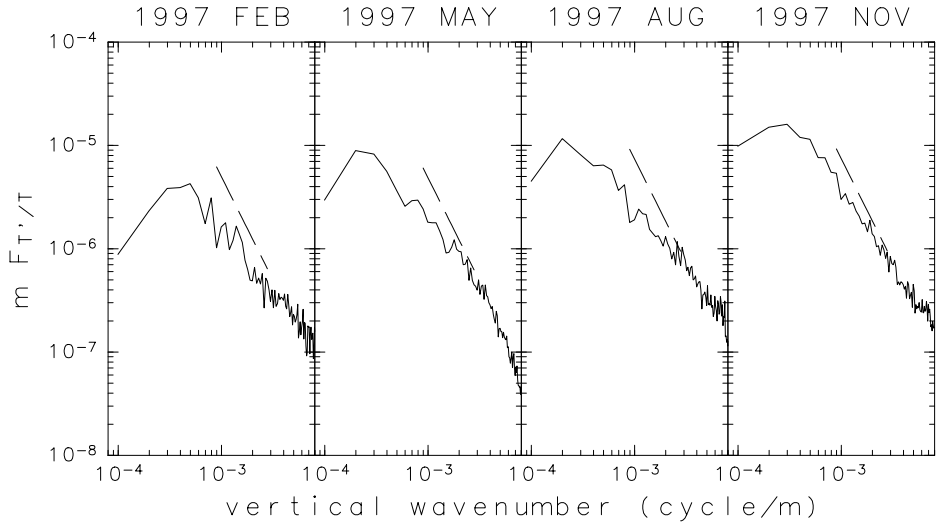

Figure 5: The monthly mean vertical wave number spectrum of normalized temperature in an energy-content form averaged in the height region of 15 – 25 km for February, May, August, and November 1997. Thin curves denote the mean spectrum, while the long-dashed lines denote the model spectrum $N^4/(10g^2m^3)$ by Smith et al. [1987].

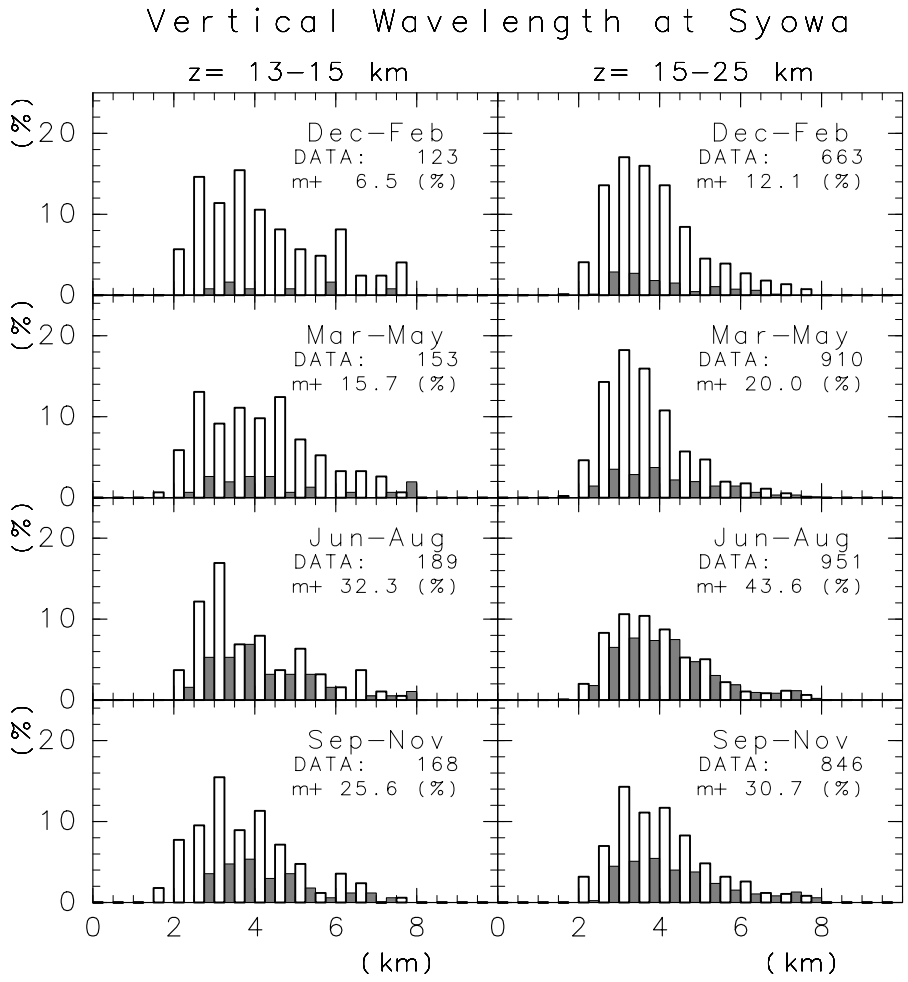

Figure 6: The probability density of gravity waves as a function of vertical wavelength. The left panels show the statistics in the height region of 13 – 15 km and the right panels the statistics in the height region of 15 – 25 km for DJF (upper panel), MAM (second panel), JJA (third panel), SON (lower panel), respectively. The open columns denote the probability density of waves transferring energy upward, and the shaded columns the probability density of waves transferring energy downward.

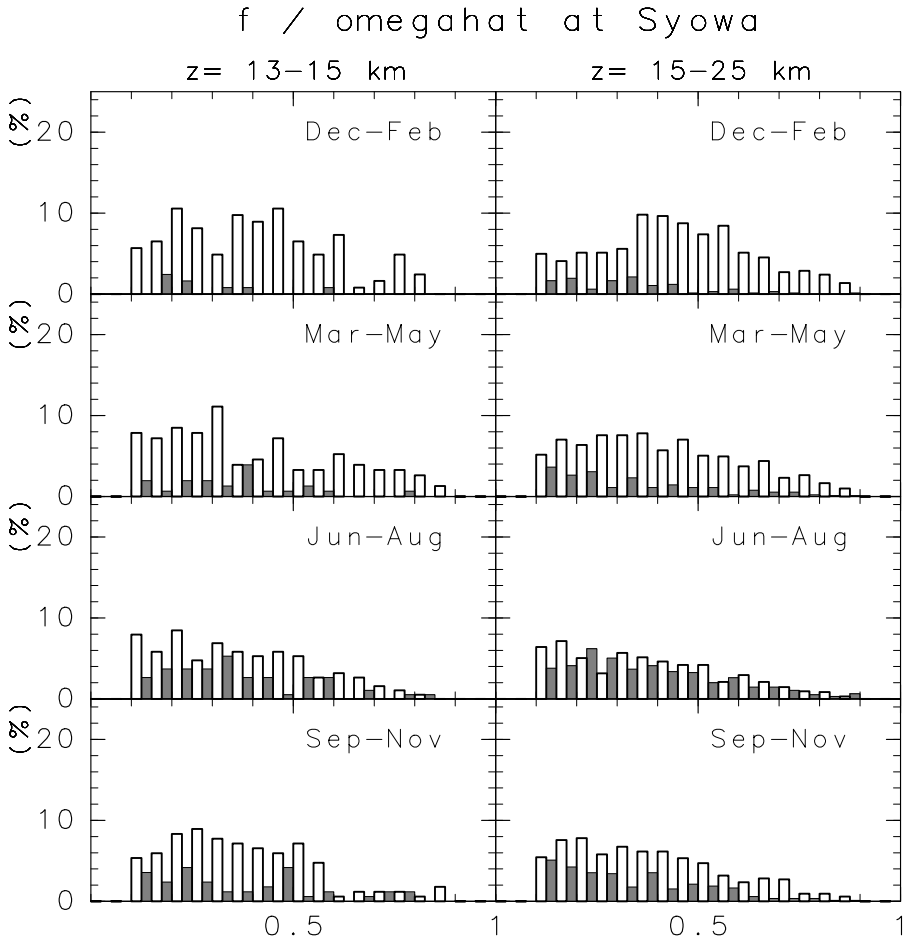

Figure 7: The same as Figure 6, buf as a function of the ratio of long to short axes of the ellipse obtained by fitting.

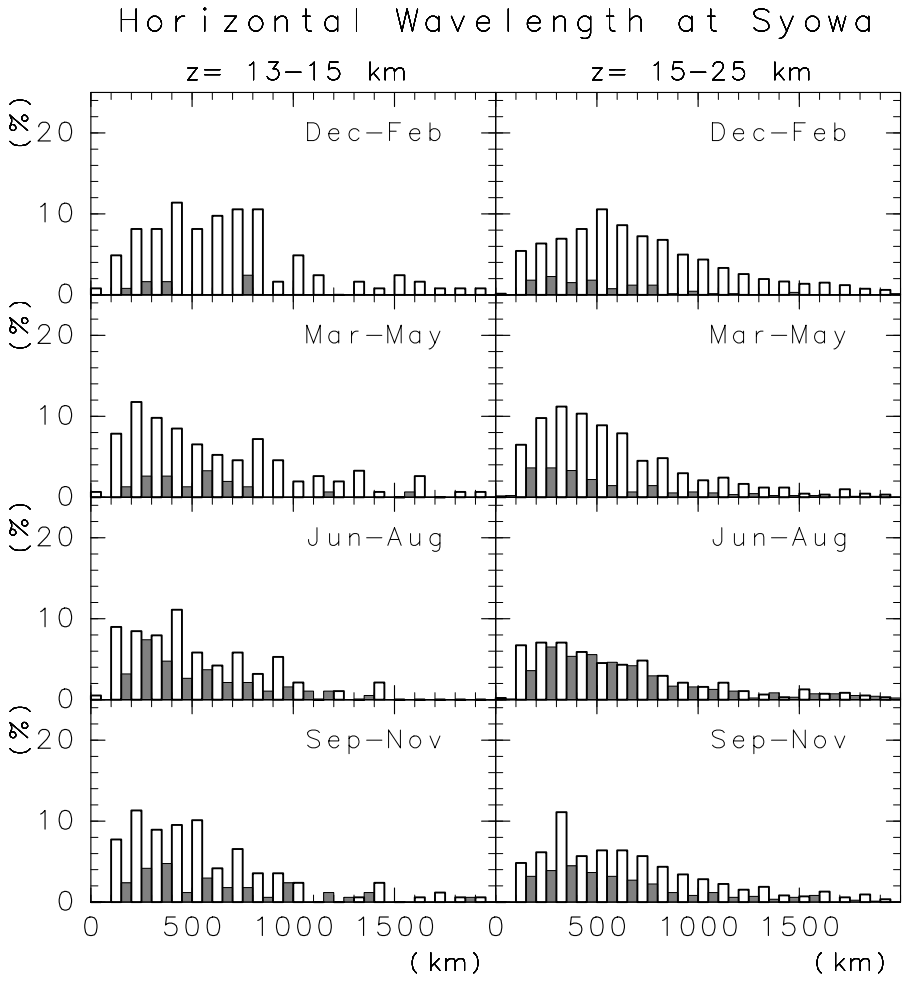

Figure 8: The same as Figure 6, but as a function of horizontal wavelength.

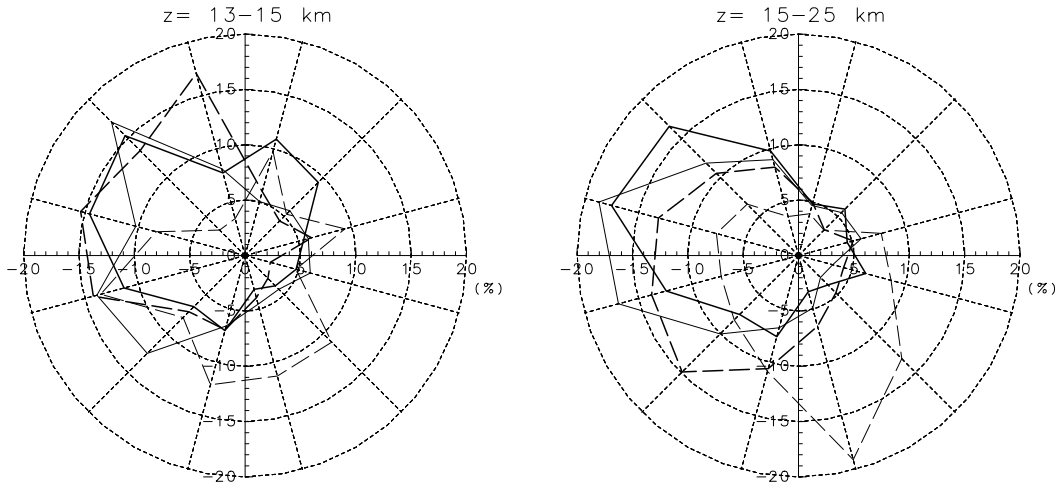

Figure 9: The probability density of gravity waves as a function of the direction of horizontal propagation relative to the mean wind in the height regions of 13–15 km (left panel) and 15–25 km (right panel). The thin dashed curves denote the probability density in summer (DJF), the thick dashed curves in autumn (MAM), the thin solid curves in winter (JJA), and the thick solid curves in Spring (SON), respectively.

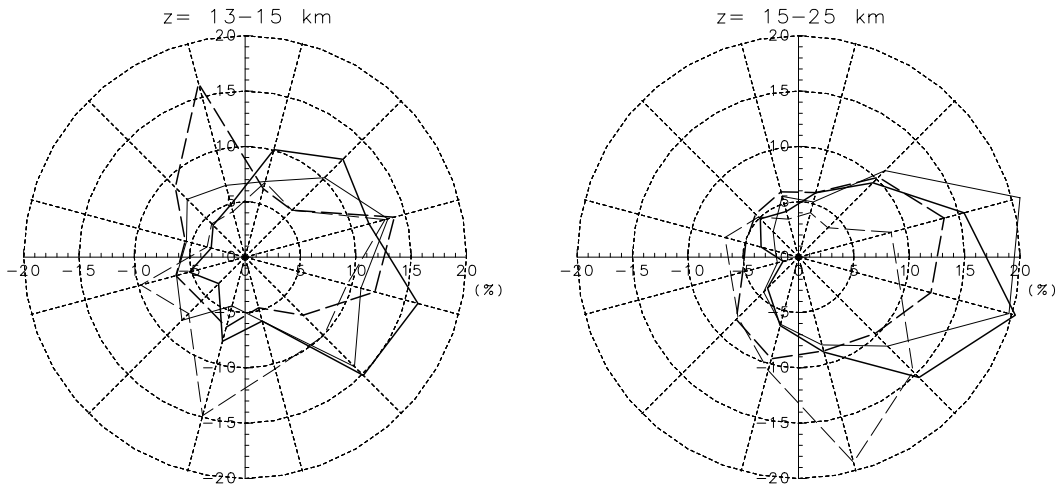

Figure 10: The same as Figure 9, but as a function of the direction of ground-based phase speed.

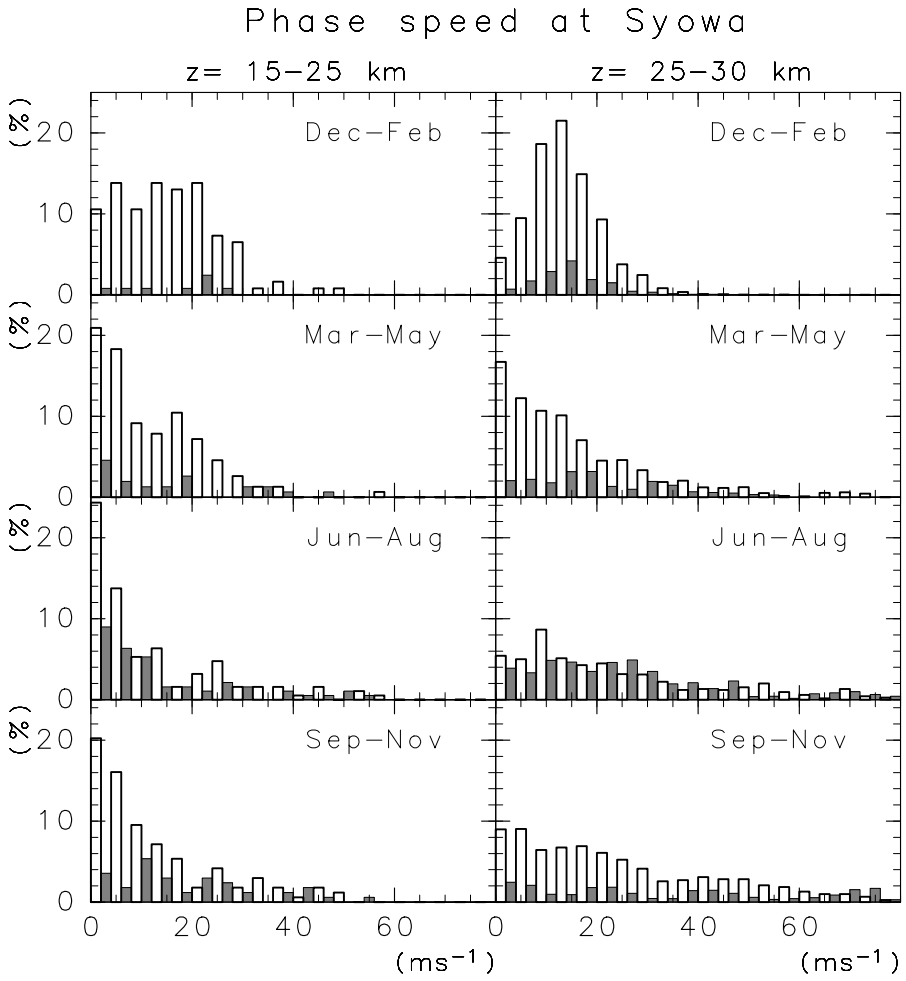

Figure 11: The same as Figure 6, but for horizontal phase speed relative to the ground.

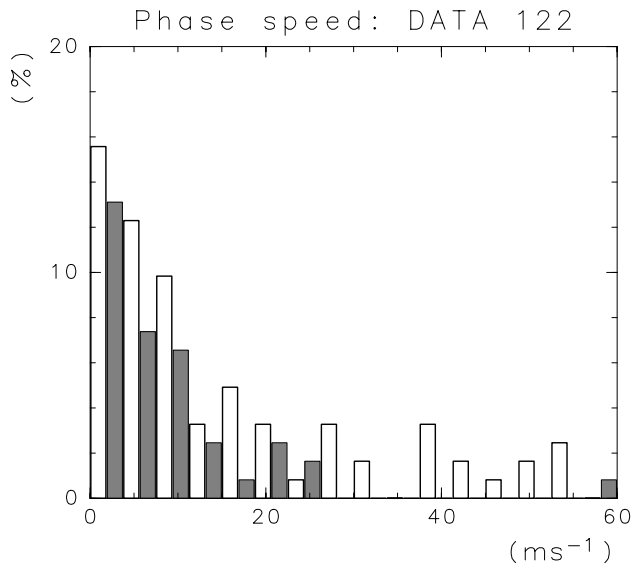

Figure 12: The probability density of gravity waves having potential energy greater than 1.5 J kg^{-1} in the height region of 13 – 15 km as a function of ground-based phase speed. Shaded and open columns denote the case when potential energy in the height region of 20 – 22 km is larger and less than 1.5 J kg^{-1}, respectively.

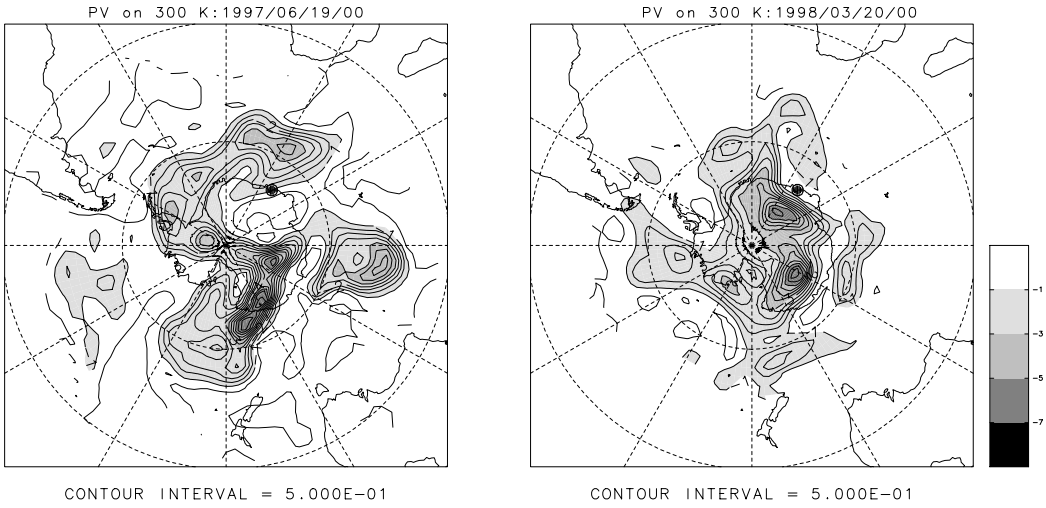

Figure 13: Potential vorticity maps on 300 Kelvin on 19 June, 1997, and 20 March, 1998, when gravity wave energy is enhanced. The closed circle denotes the location of Syowa Station. The contour interval is 0.5 PV unit.

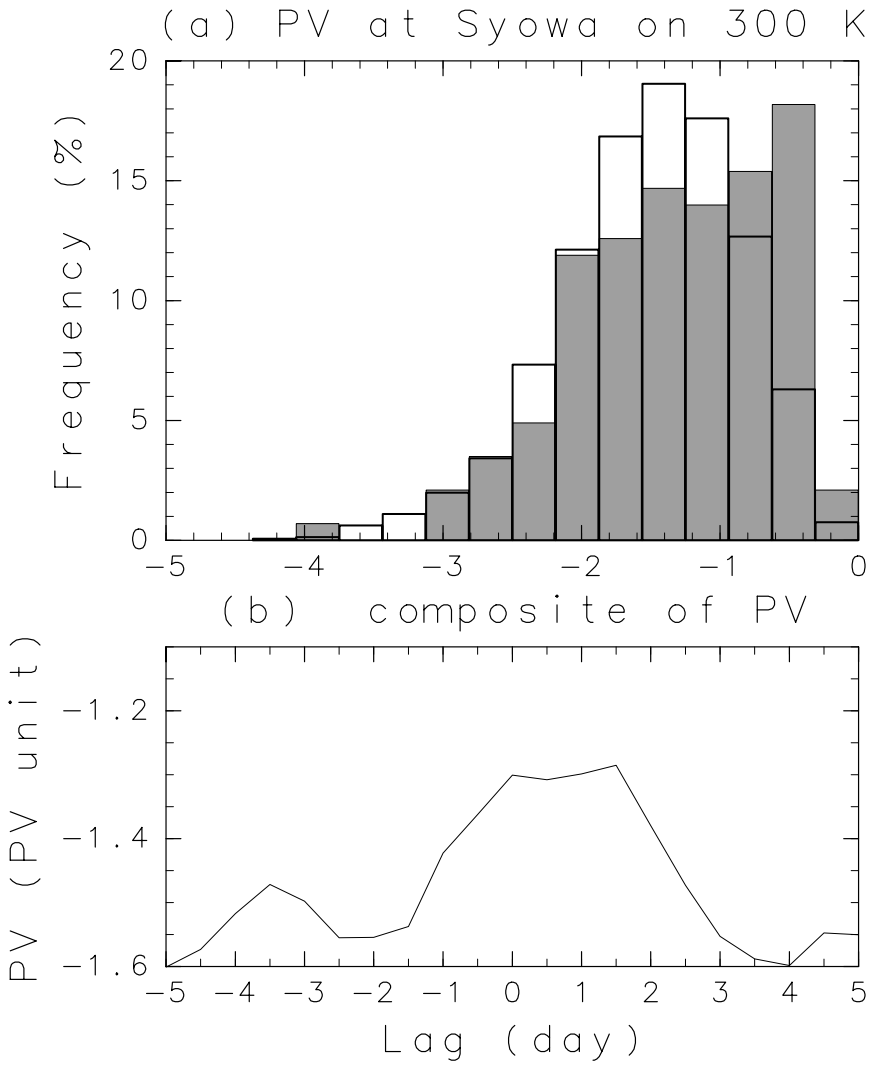

Figure 14: (a) The histogram of potential vorticity on an isentrope of 300 Kelvin at Syowa Station. The shaded columns denote the probability density of gravity waves as a function of potential vorticity whose potential energy is more than 1.5 J kg^{-1} in the height region of 13 – 15 km. The open columns denote the probability density for all period. (b) The time series of the composite of potential vorticity. The time when the potential energy of gravity waves is more than 1.5 J kg^{-1} is selected as the time lag of zero.

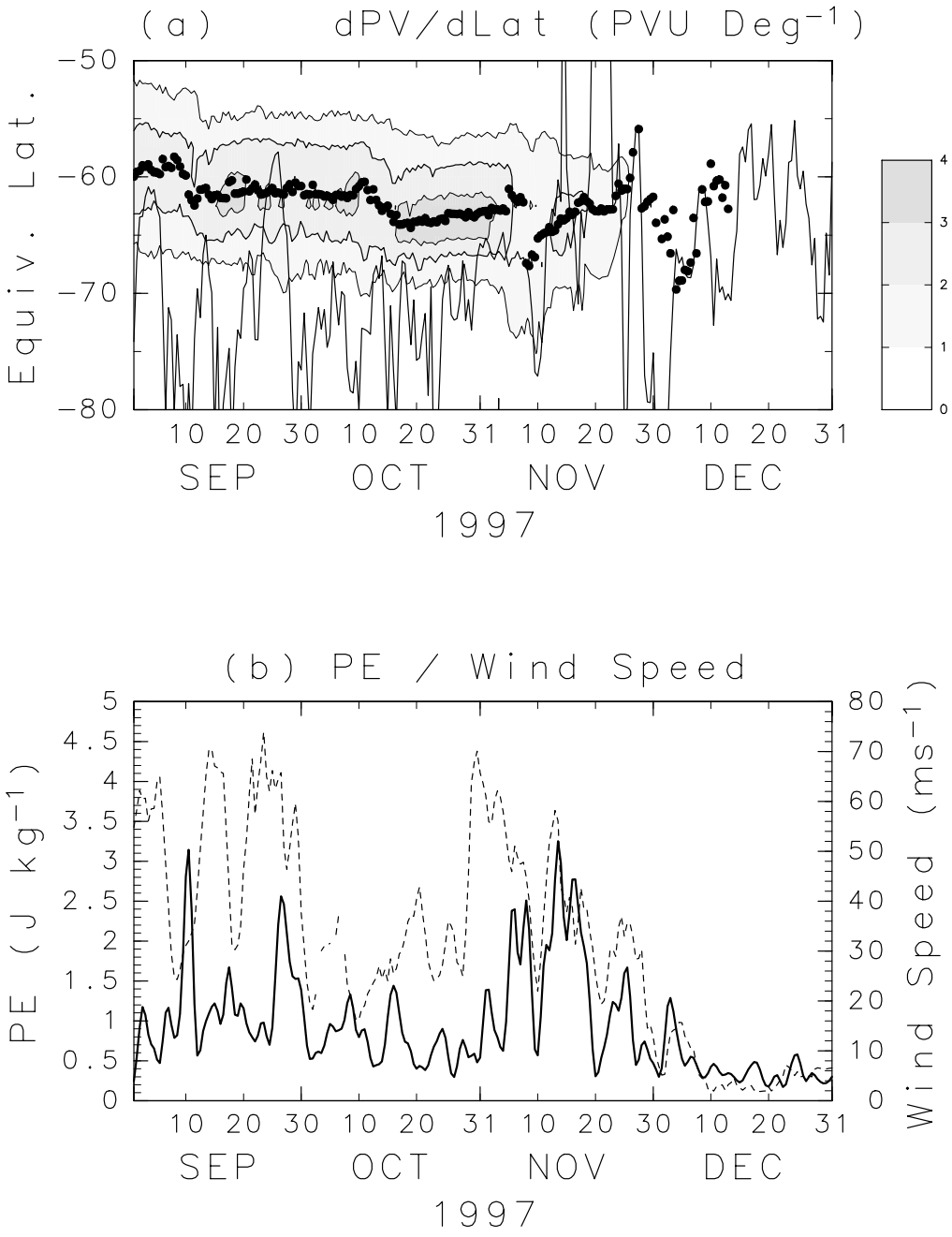

Figure 15: (a) The latitudinal gradient of potential vorticity on an isentrope of 480 Kelvin in 1997. The equivalent latitudes of the polar night jet and Syowa Station are also displayed in the closed circles and the solid curve, respectively. The contour interval is 1 PV unit deg^{-1}. (b) The time series of potential energy (solid curve) and wind speed (dashed curve) averaged in the height region of 15 – 25 km at Syowa Station in the same period. The units are J kg^{-1} and m s^{-1}.

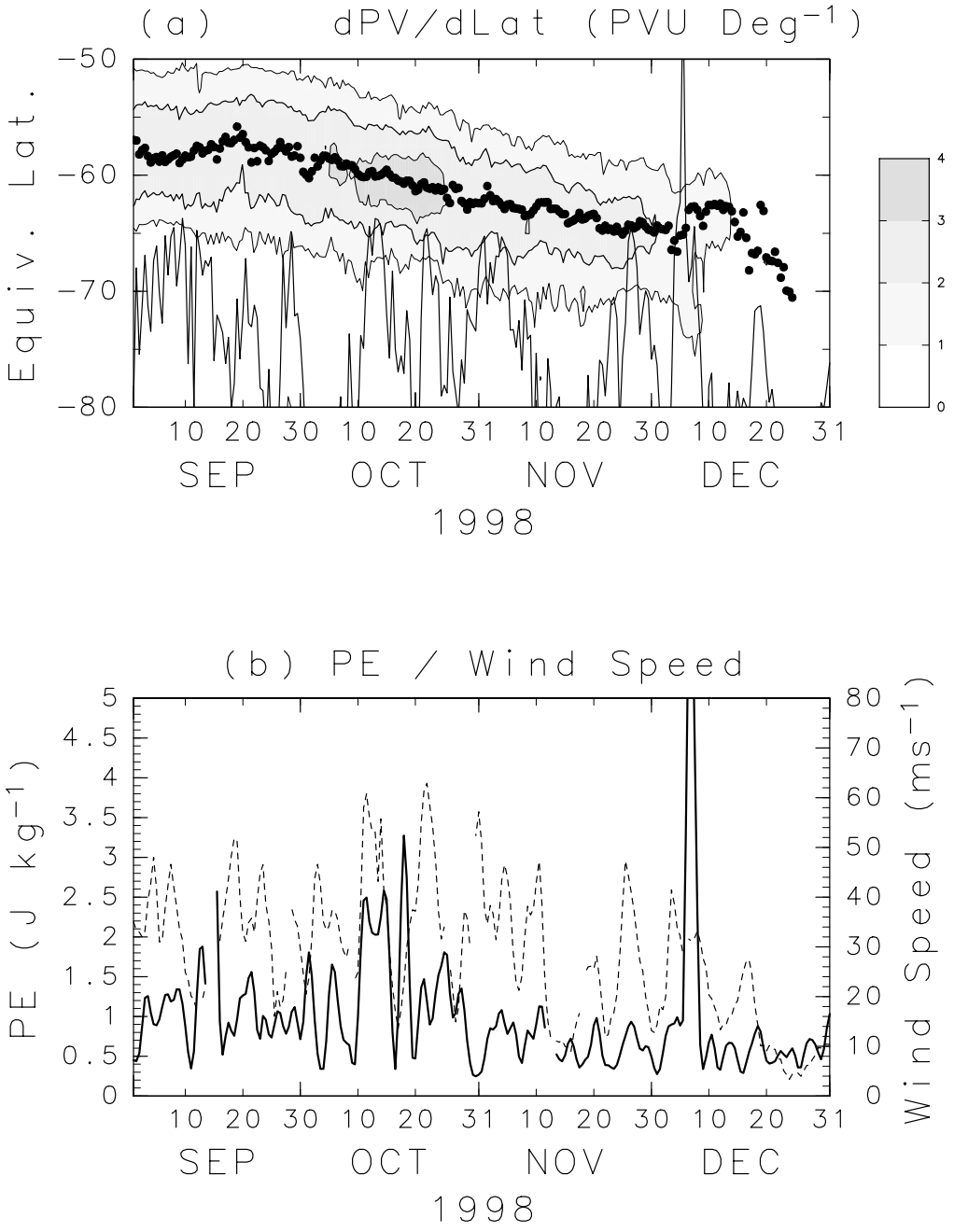

Figure 16: The same as Figure 12, but for the year of 1998.